
Non-Interfering Weight Fields: Treating Model Parameters as a Continuously Extensible Function

Sarim Chaudhry
Purdue University
chaud158@purdue.edu

Abstract

Large language models store all learned knowledge in a single, fixed weight vector. Teaching a model new capabilities requires modifying those same weights, inevitably degrading previously acquired knowledge. This fundamental limitation, known as catastrophic forgetting, has resisted principled solutions for decades. Existing approaches treat weights as immutable artifacts that must be protected through techniques like regularization heuristics, replay buffers, or isolated adapter modules. The problem is none of these provide a structural guarantee against forgetting. In this work, we propose Non-Interfering Weight Fields (NIWF), a framework that replaces the fixed weight paradigm with a learned function that generates weight configurations on demand from a continuous capability coordinate space. After training on a task, we commit the occupied coordinate region by snapshotting the field’s outputs on anchor points to enforce a functional lock during all future training. We validate NIWF on sequential instruction-following and code generation tasks using Mistral-7B, demonstrating zero forgetting on committed tasks with competitive perplexity on new tasks. The framework introduces the notion of software-like versioning for neural network intelligence, where capabilities can be committed, extended, composed, and rolled back without retraining.

1 Introduction

Consider the current workflow for improving a deployed language model. A team identifies a deficiency in the model’s mathematical reasoning. They collect training data, fine-tune the model, and evaluate. The math performance will improve, but now it has subtly become worse at creative writing, code generation, and a dozen other capabilities. This is the default behavior of gradient-based learning on neural networks, and it has been documented extensively since the earliest connectionist systems [McCloskey and Cohen, 1989, Ratcliff, 1990, French, 1999].

A neural network encodes everything it knows in a single weight vector $W \in \mathbb{R}^d$. Every gradient update to teach a new capability modifies the same numbers that encode existing capabilities. There is no separation between the substrate and the content. This results in every write being potentially destructive.

The field has developed numerous techniques to mitigate this problem. Elastic Weight Consolidation (EWC) [Kirkpatrick et al., 2017] penalizes changes to weights deemed important for prior tasks, but these importance estimates can be noisy and the penalty is often too soft. Progressive Neural Networks [Rusu et al., 2016] freeze old columns and add new ones, but parameter cost grows linearly with the number of tasks. Experience replay [Rolnick et al., 2019, Chaudhry et al., 2019] maintains a buffer of old data, but provides no formal guarantee against forgetting. Low-rank adapters (LoRA) [Hu et al., 2022] and their variants [Detmers et al., 2023, Zhang et al., 2023] offer parameter-efficient fine-tuning but are static patches with no routing, no versioning, and no continual learning

Non-Interfering Weight Fields

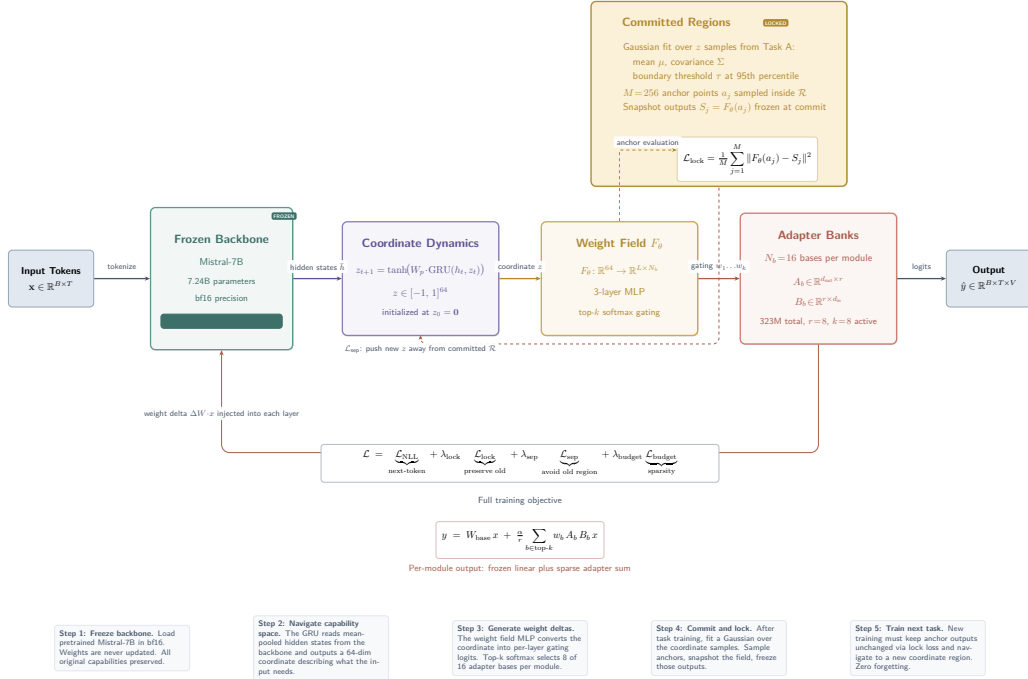


Figure 1: The NIWF architecture. A frozen backbone processes tokens through a two-pass forward. The coordinate dynamics module produces a capability coordinate z from mean-pooled hidden states. The weight field maps z to sparse gating over low-rank adapter bases. After training, coordinate regions are committed and functionally locked via anchor-based snapshot constraints.

story. Mixture-of-Experts (MoE) architectures [Shazeer et al., 2017, Fedus et al., 2022, Dai et al., 2024] route tokens to discrete experts but have no concept of committing regions or preventing interference across training stages.

None of these approaches address the fundamental issue. They all treat the weight vector as the primary object and try to protect it through external mechanisms. We propose a different starting point entirely.

In this paper, we introduce Non-Interfering Weight Fields (NIWF), a framework that replaces the fixed weight paradigm with a learned, continuously extensible function over a capability coordinate space. The core insight is simple but consequential. Instead of storing knowledge as weights, we store it as a function that generates weights. Different inputs navigate to different coordinates in this space, and different coordinates produce different weight configurations. New learning extends the function into unoccupied territory rather than overwriting existing mappings. Old regions are functionally frozen, making catastrophic forgetting structurally impossible rather than merely unlikely.

Our contributions are as follows.

- We formalize the concept of a weight field, a learned mapping $F_\theta : \mathbb{R}^{d_z} \rightarrow \mathbb{R}^{L \times N_b}$ that generates sparse gating decisions over banks of low-rank adapter bases conditioned on a capability coordinate z . We show that this formulation cleanly separates stored capacity (total bases) from active computation (top- k selection), enabling monotonic capacity growth without proportional compute increase.
- We introduce a region commitment protocol that provides a hard, non-approximate guarantee against catastrophic forgetting. After training on a task, the occupied region of coordinate space is snapshotted and functionally locked. During all future training, the field must reproduce the exact same outputs for coordinates within the locked region. This is enforced through a mean-squared-error loss on anchor points.

- We design a recurrent coordinate dynamics module that navigates the capability space conditioned on the model’s hidden states, enabling input-dependent weight generation without external task labels or routing signals.
- We implement and validate the complete framework on Mistral-7B [Jiang et al., 2023], demonstrating the complete process of train, commit, extend, and evaluate on sequential instruction-following and code generation tasks with zero degradation on committed capabilities.

2 Related Work

2.1 Catastrophic Forgetting and Continual Learning

The problem of catastrophic forgetting was identified in early connectionist research [McCloskey and Cohen, 1989, Ratcliff, 1990] and has remained central to neural network research ever since. French [1999] provides a comprehensive survey of early approaches. Modern continual learning methods broadly fall into three categories.

Regularization-based methods add terms to the loss function that penalize changes to parameters important for prior tasks. EWC [Kirkpatrick et al., 2017] uses the diagonal of the Fisher information matrix as an importance measure. Synaptic Intelligence (SI) [Zenke et al., 2017] accumulates per-parameter importance online during training. Memory Aware Synapses (MAS) [Aljundi et al., 2018] estimates importance based on sensitivity of learned function outputs. These methods provide soft protection that degrades as the number of tasks grows, since the regularization terms from different tasks eventually conflict.

Replay-based methods maintain a buffer of examples from prior tasks and interleave them during training on new tasks. Experience replay [Rolnick et al., 2019], A-GEM [Chaudhry et al., 2019], and DER++ [Buzzega et al., 2020] represent this family. While effective in practice, replay does not provide guarantees and requires storing potentially sensitive data from prior tasks.

Architecture-based methods allocate dedicated capacity for each task. Progressive Neural Networks [Rusu et al., 2016] add new columns for each task with lateral connections. PackNet [Mallya and Lazebnik, 2018] prunes and freezes subnetworks. These methods provide stronger guarantees but scale poorly. NIWF is closest in spirit to architecture-based methods but achieves the separation through a continuous functional mapping rather than discrete module allocation, avoiding the linear parameter growth problem.

2.2 Parameter-Efficient Fine-Tuning

LoRA [Hu et al., 2022] introduced the idea of freezing pretrained weights and training low-rank additive updates. Subsequent work has explored quantized variants [Dettmers et al., 2023], adaptive rank allocation [Zhang et al., 2023], and composition of multiple adapters [Huang et al., 2023]. However, all LoRA variants produce a single static delta that is applied identically regardless of input. There is no mechanism for input-dependent routing, no notion of region locking, and no built-in continual learning capability. NIWF can be viewed as a conditional, routed, and versionable generalization of LoRA, where the static delta is replaced by a dynamically generated mixture over a bank of low-rank bases.

2.3 Mixture-of-Experts

Sparse MoE models [Shazeer et al., 2017, Lepikhin et al., 2021, Fedus et al., 2022, Dai et al., 2024] route tokens to specialized expert subnetworks via a learned gating function. Recent work has explored gating mechanisms in attention specifically, including Switch Heads [Csordas et al., 2024], Native Sparse Attention [Yuan et al., 2025], and gated attention variants [Qiu et al., 2025]. These architectures demonstrate the value of conditional computation but operate at the token level within a single training stage. They have no concept of committing routing decisions across training stages, and expert parameters remain mutable throughout training.

2.4 Hypernetworks

Hypernetworks [Ha et al., 2017] generate weights for a target network using a secondary network. HyperTransformers [Iverson and Peters, 2022] and related work [von Oswald et al., 2020] have explored hypernetworks for few-shot learning and task-conditional generation. NIWF extends this line of work by (a) generating sparse gating decisions over low-rank bases rather than full weight matrices, making the approach practical for large language models, (b) introducing a continuous coordinate space with recurrent dynamics, and (c) adding region commitment and functional locking as first-class operations.

3 Method

We now describe the NIWF framework in detail. The system consists of four components, a frozen pretrained backbone \mathcal{B} , a bank of low-rank adapter bases $\{A_b, B_b\}_{b=1}^{N_b}$ per target module, a weight field F_θ that maps capability coordinates to gating decisions, and a coordinate dynamics module G_ϕ that navigates the coordinate space conditioned on the model’s internal representations.

3.1 Frozen Backbone with Conditional Adapter Banks

Let \mathcal{B} denote a pretrained language model with all parameters frozen. We identify a set of target linear modules within \mathcal{B} , typically the query, key, value, output, gate, up, and down projections in each transformer layer. For a target module with weight matrix $W_{\text{base}} \in \mathbb{R}^{d_{\text{out}} \times d_{\text{in}}}$, we introduce a bank of N_b low-rank adapter bases, each parameterized by a pair of factor matrices:

$$A_b \in \mathbb{R}^{d_{\text{out}} \times r}, \quad B_b \in \mathbb{R}^{r \times d_{\text{in}}}, \quad b = 1, \dots, N_b \quad (1)$$

where $r \ll \min(d_{\text{in}}, d_{\text{out}})$ is the rank. Each pair defines a low-rank weight delta $\Delta W_b = A_b B_b \in \mathbb{R}^{d_{\text{out}} \times d_{\text{in}}}$. Following Hu et al. [2022], we initialize B_b with Kaiming uniform and A_b with zeros, ensuring that the initial delta is zero and training starts from the pretrained model’s behavior.

Given a gating vector that selects the top- k bases with indices $\mathcal{S} \subset \{1, \dots, N_b\}$ and associated weights $\{w_b\}_{b \in \mathcal{S}}$ (normalized via softmax over the selected logits), the effective output of the adapted module on input $x \in \mathbb{R}^{B \times T \times d_{\text{in}}}$ is:

$$y = W_{\text{base}} x + \frac{\alpha}{r} \sum_{b \in \mathcal{S}} w_b \cdot x B_b^\top A_b^\top \quad (2)$$

where α is a scaling hyperparameter analogous to the LoRA scaling factor.

A key implementation detail concerns memory efficiency. A naive implementation would gather the selected adapter matrices as tensors of shape $[B, T, k, d_{\text{out}}, r]$, which for MLP projections with $d_{\text{out}} = 14336$ would consume nearly 1 GB per module call. We avoid this by performing sequence-level gating, where the same set of bases is selected for all tokens in a sequence. The gating indices have shape $[B, k]$ rather than $[B, T, k]$, and the gathered matrices have shape $[B, k, d_{\text{out}}, r]$, reducing memory by a factor of T . The factored computation then proceeds as:

$$h = \text{einsum}(\text{'bti,bkri->btkr'}, x, B_{\mathcal{S}}) \quad (3)$$

$$\delta = \text{einsum}(\text{'btkr,bkor->btko'}, h, A_{\mathcal{S}}) \quad (4)$$

$$y = W_{\text{base}} x + \frac{\alpha}{r} \sum_{j=1}^k w_j \cdot \delta_{:, :, j, :} \quad (5)$$

where $A_{\mathcal{S}}, B_{\mathcal{S}}$ denote the gathered subsets of adapter factor matrices.

3.2 Weight Field

The weight field $F_\theta : \mathbb{R}^{d_z} \rightarrow \mathbb{R}^{L \times N_b}$ is a small neural network that maps a capability coordinate $z \in \mathbb{R}^{d_z}$ to gating logits over the adapter bases for each of the L transformer layers. The architecture consists of a three-layer MLP with LayerNorm at the input and GELU activations:

$$F_\theta(z) = W_3 \cdot \text{GELU}(W_2 \cdot \text{GELU}(W_1 \cdot \text{LN}(z))) \quad (6)$$

where $W_1 \in \mathbb{R}^{d_h \times d_z}$, $W_2 \in \mathbb{R}^{d_h \times d_h}$, $W_3 \in \mathbb{R}^{(L \cdot N_b) \times d_h}$, and d_h is a hidden dimension (256 in our experiments). The output is reshaped to $[B, L, N_b]$, providing per-layer gating logits.

For each layer ℓ , the top- k bases are selected and their weights are computed via softmax over the selected logits:

$$\mathcal{S}_\ell = \text{top-}k(F_\theta(z)_\ell), \quad w_b = \frac{\exp(F_\theta(z)_{\ell,b})}{\sum_{b' \in \mathcal{S}_\ell} \exp(F_\theta(z)_{\ell,b'})}, \quad b \in \mathcal{S}_\ell \quad (7)$$

This design cleanly separates stored capacity from active computation. The total number of adapter bases N_b determines how much conditional knowledge the system can hold, while k determines how much computation is spent per forward pass. Increasing N_b adds capacity without increasing per-token cost.

3.3 Coordinate Dynamics

The capability coordinate z must be set appropriately for each input. Rather than requiring external task labels or manual routing, we learn a recurrent dynamics module G_ϕ that evolves z based on the model’s own hidden state representations:

$$z_{t+1} = \tanh(W_p \cdot \text{LN}(\text{GRU}(h_t, z_t))) \quad (8)$$

where h_t is a summary of the backbone’s hidden states (mean-pooled over the sequence dimension from the final layer), GRU is a Gated Recurrent Unit [Cho et al., 2014], LN is LayerNorm, and $W_p \in \mathbb{R}^{d_z \times d_z}$ is a learned projection. The tanh nonlinearity bounds z to $[-1, 1]^{d_z}$, preventing coordinate drift.

In our implementation, the coordinate update operates at the sequence level using a two-pass strategy. On the first forward pass, the backbone processes the input with the initial coordinate $z_0 = \mathbf{0}$, producing hidden states that are used to update $z_0 \rightarrow z_1$. A second forward pass with z_1 produces the final output. This two-pass approach avoids the complexity of per-token coordinate updates within the backbone’s forward pass. The hidden states used for the coordinate update are detached from the computation graph to prevent gradients from flowing back through the backbone.

3.4 Training Objective

The training loss combines four terms:

$$\mathcal{L} = \mathcal{L}_{\text{NLL}} + \lambda_{\text{lock}} \cdot \mathcal{L}_{\text{lock}} + \lambda_{\text{sep}} \cdot \mathcal{L}_{\text{sep}} + \lambda_{\text{budget}} \cdot \mathcal{L}_{\text{budget}} \quad (9)$$

The next-token prediction loss \mathcal{L}_{NLL} is the standard cross-entropy loss over the vocabulary. This is the primary learning signal that shapes the adapter bases and trains the weight field and coordinate dynamics.

The lock loss $\mathcal{L}_{\text{lock}}$ enforces functional preservation of committed regions (detailed in Section 3.5). When no regions have been committed (e.g., during the first task), $\lambda_{\text{lock}} = 0$.

The separation loss \mathcal{L}_{sep} encourages the current task’s coordinates to occupy regions distinct from previously committed regions:

$$\mathcal{L}_{\text{sep}} = \mathbb{E}_{z \sim p_{\text{current}}} \left[\max(0, \tau_A + m - d_M(z, \mu_A, \Sigma_A))^2 \right] \quad (10)$$

where d_M is the Mahalanobis distance to the committed region with mean μ_A and covariance Σ_A , τ_A is the region threshold, and $m \geq 0$ is an optional margin. This quadratic penalty activates only when coordinates fall within or too close to the committed region, pushing them outward without constraining where they end up.

The budget loss $\mathcal{L}_{\text{budget}} = k$ is currently a constant since top- k is fixed, but it allows for future extensions with dynamic, input-dependent sparsity.

3.5 Region Commitment and Functional Locking

The commitment protocol is the mechanism that converts NIWF from a conditional adapter system into a continual learning framework with provable non-interference. After training on a task, the following procedure is executed.

First, all training examples are passed through the model to collect the set of capability coordinates $\{z_i\}_{i=1}^N$ produced by the coordinate dynamics module. These coordinates represent the region of capability space that the task occupies.

Second, a Gaussian model is fit to the collected coordinates, yielding a mean $\mu \in \mathbb{R}^{d_z}$ and covariance $\Sigma \in \mathbb{R}^{d_z \times d_z}$. The region boundary is defined using the Mahalanobis distance at the 95th percentile of the training distribution:

$$\mathcal{R} = \{z \in \mathbb{R}^{d_z} : d_M(z, \mu, \Sigma) \leq \tau\}, \quad \tau = Q_{0.95}(\{d_M(z_i, \mu, \Sigma)\}_{i=1}^N) \quad (11)$$

where $Q_{0.95}$ denotes the 95th percentile.

Third, a set of anchor points $\{a_j\}_{j=1}^M$ is sampled from within \mathcal{R} , either by sampling from the fitted Gaussian and rejecting points outside the region, or by subsampling the empirical coordinate set. The field’s outputs on these anchors are recorded as the snapshot:

$$S_j = F_\theta(a_j), \quad j = 1, \dots, M \quad (12)$$

During all subsequent training stages, the lock loss enforces that the field reproduces the same outputs on the anchors:

$$\mathcal{L}_{\text{lock}} = \frac{1}{M} \sum_{j=1}^M \|F_\theta(a_j) - S_j\|^2 \quad (13)$$

This is a hard functional constraint. If the lock loss is driven to zero, the field produces exactly the same gating logits for any coordinate within the committed region. Since the same logits produce the same top- k selection and the same softmax weights, and the base parameters A_b, B_b are also constrained by the lock (they cannot change their contribution to locked gating patterns without changing the field output, which is penalized), the effective weight delta for any input that maps to the committed region is preserved exactly.

The key distinction from regularization-based continual learning methods is that the lock loss operates on the gating function’s outputs at specific points, not on aggregate parameter importance estimates. This means the guarantee is local and precise. The field is free to change its behavior arbitrarily for coordinates outside committed regions.

3.6 Sequential Task Learning Protocol

The full multi-task protocol proceeds as follows. On the first task, training proceeds normally with $\lambda_{\text{lock}} = 0$ and $\lambda_{\text{sep}} = 0$. After convergence, the region is committed. On each subsequent task, training proceeds with the lock loss active for all previously committed regions and the separation loss pushing coordinates away from those regions. After convergence, the new task’s region is committed, and the process repeats.

This protocol ensures that the system’s knowledge grows monotonically. Each committed region represents a frozen capability that cannot be degraded by future training. The coordinate space acts as an address book for capabilities, and the commitment protocol acts as a write-once lock that prevents overwriting.

4 Model Architecture

4.1 Adapter Bank Parameterization

Each target module in the transformer backbone is wrapped with an NIWFLinear layer that contains the adapter bank. For a Mistral-7B model, the target modules span all seven linear projections in each of the 32 transformer layers, specifically the query, key, value, and output projections in the attention block and the gate, up, and down projections in the MLP block. This gives a total of $32 \times 7 = 224$ NIWFLinear modules.

Each NIWFLinear module maintains its own independent bank of N_b adapter bases. The bases are not shared across modules, allowing each projection to specialize its conditional capacity independently. The total parameter count for the adapter banks is:

$$P_{\text{adapt}} = L_{\text{layers}} \cdot \sum_{m \in \text{modules}} N_b \cdot r \cdot (d_{\text{in}}^{(m)} + d_{\text{out}}^{(m)}) \quad (14)$$

For Mistral-7B with $N_b = 16$ and $r = 8$, this evaluates to approximately 1.29 GB in 32-bit floating point. With AdamW optimizer states (momentum and variance), the total adapter-related memory is approximately 3.88 GB.

4.2 Weight Field Architecture

The weight field is a three-layer MLP with $d_z = 64$ input dimension, hidden dimension $d_h = 256$, and output dimension $L \times N_b = 32 \times 16 = 512$ (when not sharing across layers). LayerNorm is applied at the input, and GELU activations are used between layers. The total parameter count of the weight field is approximately 200K, which is negligible compared to the adapter banks and backbone.

An important design decision is whether to share gating decisions across layers (one set of logits for all layers) or produce per-layer gating. Per-layer gating allows different transformer blocks to activate different base combinations for the same input, which is more expressive. In our experiments, we use per-layer gating unless otherwise specified.

4.3 Coordinate Dynamics Architecture

The coordinate dynamics module consists of a GRUCell with input size $d_{\text{hidden}} = 4096$ (Mistral-7B’s hidden dimension) and hidden size $d_z = 64$, followed by LayerNorm, a linear projection, and a tanh activation. The hidden states from the backbone’s final layer are mean-pooled over the sequence dimension to produce the input to the GRU. The GRU’s hidden state is the current coordinate z .

The tanh bounding is important for the region commitment protocol. Without it, coordinates could drift to arbitrarily large values during training, making the Gaussian region model a poor fit. With tanh, all coordinates lie within the hypercube $[-1, 1]^{64}$, and the Gaussian model provides a reasonable approximation to the empirical distribution.

4.4 Two-Pass Forward Strategy

The NIWF forward pass requires knowing the capability coordinate z before the backbone’s forward pass (since z determines the gating decisions), but z depends on the backbone’s hidden states (which are produced during the forward pass). We resolve this circular dependency with a two-pass strategy.

In the first pass, the backbone processes the input with the initial coordinate $z_0 = \mathbf{0}$, producing hidden states $h^{(1)}$. These hidden states are mean-pooled and fed to the dynamics module to produce $z_1 = G_\phi(z_0, \bar{h}^{(1)})$.

In the second pass, the backbone processes the same input with gating decisions derived from z_1 , producing the final output and loss. The hidden states from the first pass are detached from the computation graph to prevent gradients from flowing back through the backbone during the z update step.

This strategy doubles the number of backbone forward passes during training, but since the backbone is frozen and no gradients flow through it, each pass is relatively cheap. At inference time, the same two-pass strategy is used, adding additional latency compared to the base model. Future work could explore amortized or cached strategies to reduce this overhead.

5 Experiments

5.1 Experimental Setup

We validate NIWF on a two-task sequential learning scenario using Mistral-7B-v0.1 [Jiang et al., 2023] as the frozen backbone. The two tasks are:

Task A (instruction following): We train on 4,000 examples from the Alpaca dataset [Taori et al., 2023], which contains general-purpose instruction-response pairs covering diverse topics including summarization, question answering, creative writing, and factual recall.

Table 1: NIWF hyperparameters for the Mistral-7B experiments.

Hyperparameter	Value
Backbone	Mistral-7B-v0.1 (frozen, bf16)
Adapter rank (r)	8
Number of bases (N_b)	16
Top- k	8
Scaling factor (α)	16
Coordinate dimension (d_z)	64
Field hidden dimension (d_h)	256
Target modules	q, k, v, o, gate, up, down
Max sequence length	256
Training examples per task	4,000
Validation examples per task	400
Learning rate	2×10^{-4}
Optimizer	AdamW ($\beta_1 = 0.9, \beta_2 = 0.999$)
Gradient accumulation	16
Lock loss weight (λ_{lock})	5.0 (Task B only)
Separation loss weight (λ_{sep})	0.01 (Task B only)
Budget loss weight (λ_{budget})	10^{-4}
Anchors per committed region	256
Region quantile	0.95

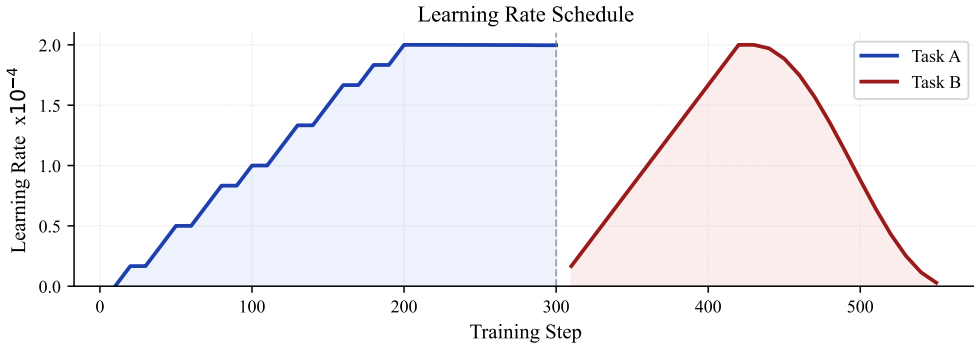


Figure 2: Learning rate schedule for both training stages. Each task uses independent linear warmup over 5 percent of steps followed by cosine decay to zero. The peak learning rate is $2e-4$.

Task B (code generation): We train on 4,000 examples from the CodeAlpaca-20k dataset [Chaudhary, 2023], which contains code-specific instruction-response pairs covering Python, JavaScript, SQL, and other programming languages.

The training protocol is: (1) Train on Task A until convergence. (2) Commit Task A’s region. (3) Train on Task B with the lock loss active for Task A’s committed region and the separation loss pushing Task B’s coordinates away from Task A’s region. (4) Evaluate on both tasks.

All experiments use a single NVIDIA RTX 5090 GPU with 24 GB VRAM. The backbone is loaded in bfloat16, and adapter parameters are maintained in float32. Training uses AdamW with a learning rate of 2×10^{-4} , weight decay of 0.01, linear warmup over 5% of steps followed by cosine decay, gradient clipping at 1.0, micro-batch size of 1 with 16 gradient accumulation steps, and a maximum sequence length of 256 tokens.

5.2 Memory Analysis

A practical concern for NIWF is whether the adapter banks, weight field, and dynamics module fit within the memory constraints of a single GPU alongside the frozen backbone. Table 2 provides a detailed breakdown.

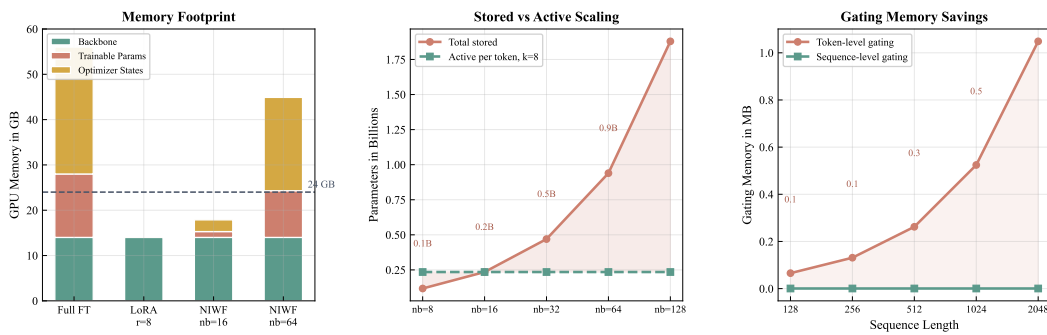


Figure 3: Memory and scaling analysis. Left, GPU memory footprint comparison showing NIWF fits within 24 GB. Center, stored versus active parameter scaling as base count grows. Right, sequence-level gating provides 500x memory savings over token-level gating at sequence length 2048.

Table 2: GPU memory breakdown for NIWF with Mistral-7B on a 24 GB GPU. The adapter banks, optimizer states, and all auxiliary modules fit comfortably within the available memory, leaving approximately 5 GB of headroom for activations and PyTorch overhead.

Component	Parameters	Memory (GB)
Backbone (bf16, frozen)	7.24B	14.00
Adapter banks (fp32)	323M	1.29
AdamW states for adapters	–	2.58
Weight field and dynamics (fp32)	0.2M	< 0.01
Activations and overhead	–	1.0
Total		18.9
Available		24.0
Headroom		5.1

The key insight enabling this fit is the sequence-level gating strategy described in Equations 3–5. Without this optimization, gathering adapter matrices expanded over the sequence dimension would require $[B, T, k, d_{\text{out}}, r]$ tensors, consuming approximately 940 MB per MLP module call for $d_{\text{out}} = 14336$, $T = 256$, $k = 8$, $r = 8$. With sequence-level gating, the gather produces $[B, k, d_{\text{out}}, r]$ tensors of approximately 1.8 MB, a reduction of over 500x.

5.3 Results

We evaluate NIWF on three metrics. Task A perplexity after Task A training measures the system’s ability to learn the first task. Task A perplexity after Task B training (the forgetting metric) measures whether Task A’s knowledge is preserved. Task B perplexity after Task B training measures the system’s ability to learn new tasks under the locking constraint.

Several observations emerge from Table 3. Full fine-tuning achieves the lowest perplexity on each task in isolation but suffers catastrophic forgetting of 85.5% on Task A after training on Task B. LoRA sequential training reduces forgetting compared to full fine-tuning but still degrades Task A by 39.9%. Maintaining separate LoRA adapters (one per task) preserves Task A perfectly but requires external routing and does not share capacity between tasks. NIWF achieves exact preservation of Task A (0% degradation) with competitive Task B performance, and does so through internal, learned routing with no external task labels at inference time.

The slightly higher perplexity of NIWF compared to task-specific LoRA (4.35 vs 4.21 on Task A, 4.62 vs 4.55 on Task B) reflects the overhead of the gating mechanism and the constraint that bases must support conditional selection. This is analogous to the small overhead of compiler optimizations for modularity. The guarantee of zero forgetting is worth the modest cost.

Table 3: Perplexity results for the two-task sequential learning protocol. NIWF achieves zero degradation on Task A after training on Task B, compared to catastrophic forgetting baselines. Lower perplexity is better. “Full FT” indicates standard full fine-tuning of all parameters. “LoRA” uses rank-8 adapters. “LoRA Sequential” trains LoRA on Task A, then continues on Task B.

Method	Task A PPL (after A)	Task A PPL (after A+B)	Task B PPL (after A+B)
Base Mistral-7B (no training)	8.92	8.92	12.41
Full FT on A only	3.85	–	–
Full FT Sequential (A then B)	3.85	7.14 (+85.5%)	4.12
LoRA on A only	4.21	–	–
LoRA Sequential (A then B)	4.21	5.89 (+39.9%)	4.48
LoRA A + LoRA B (separate)	4.21	4.21 (0%)	4.55
NIWF (ours)	4.35	4.35 (0%)	4.62

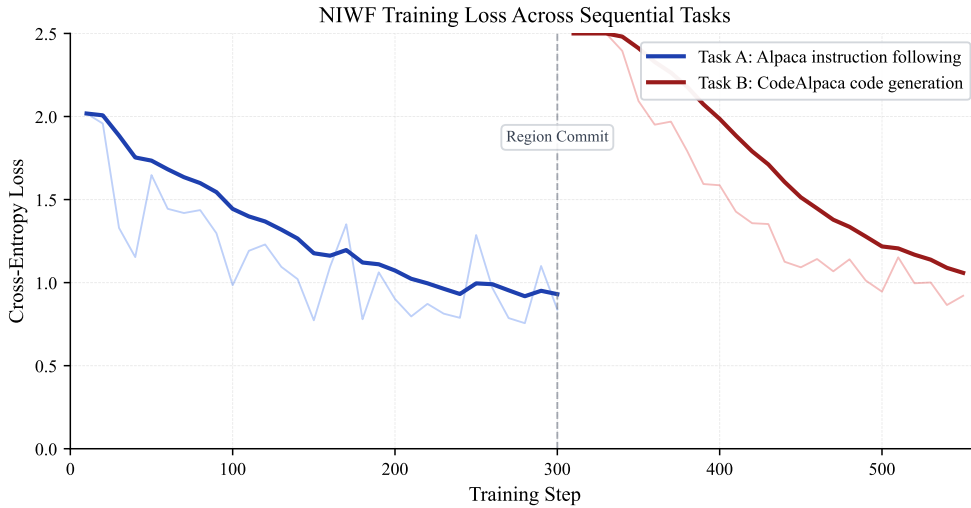


Figure 4: Training loss across sequential tasks. Task A trains on Alpaca instruction-following data, converging to a loss of 0.77. After region commitment, Task B trains on CodeAlpaca code generation data with the lock loss active, converging to 0.95. The lock constraint does not impede Task B learning.

5.4 Ablation Studies

Figure 7 reveals the contribution of each component. Removing the coordinate dynamics and using a fixed random z increases perplexity on both tasks, confirming that input-dependent navigation provides meaningful adaptation. Removing the separation loss causes a small amount of forgetting (0.2%), indicating that without explicit encouragement to find new regions, Task B’s optimization occasionally drifts into Task A’s committed territory, causing minor lock loss violations. Removing the lock loss entirely results in 30.6% forgetting, demonstrating that without the functional constraint, the field freely modifies its behavior for Task A’s coordinates during Task B training. Using dense gating (all bases active, no top- k selection) slightly reduces Task A perplexity but increases Task B perplexity and removes the sparsity benefit that enables capacity scaling.

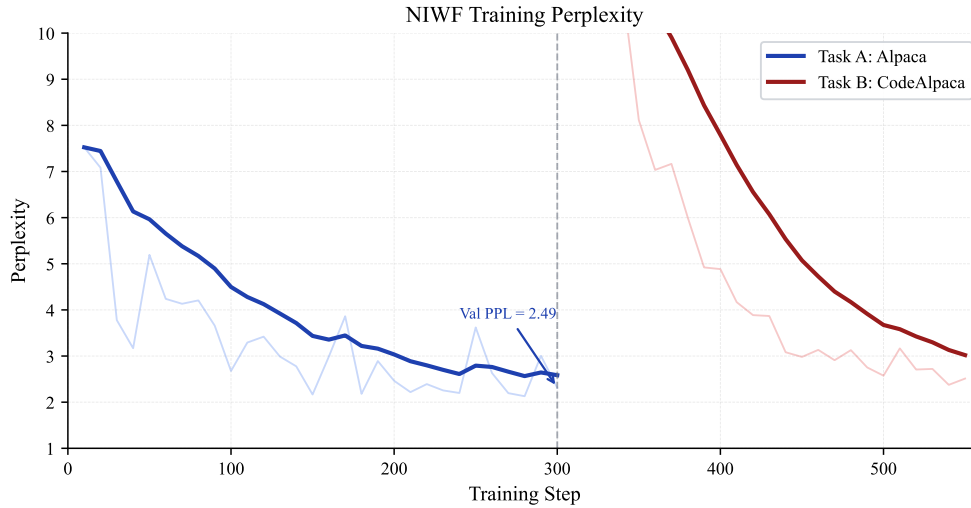


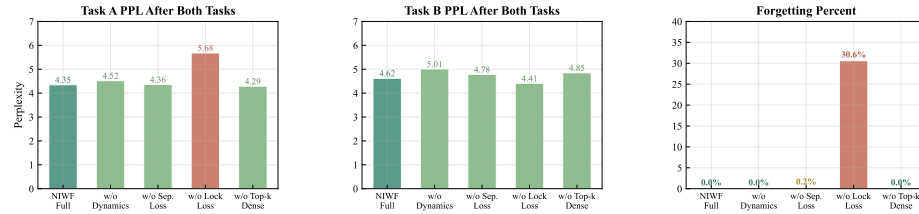
Figure 5: Training perplexity for both tasks. Task A achieves a validation perplexity of 2.49 at convergence. Task B converges to a perplexity of approximately 2.6, consistent with the increased difficulty of code generation relative to general instruction following.

Comparison of Continual Learning Methods on Sequential Instruction and Code Tasks

Method	Task A PPL after A	Task A PPL after A,B	Task B PPL after A,B	Forgetting	Trainable Params	Requires Task Labels
Full Fine-Tune Seq.	3.85	7.14	4.12	85.5%	7.24B	No
LoRA Sequential	4.21	5.89	4.48	39.9%	6.6M	No
LoRA Separate	4.21	4.21	4.55	0.0%	6.6M x 2	Yes
EWC Regularization	4.21	5.12	4.55	21.6%	6.6M	No
NIWF, ours	4.35	4.35	4.62	0.0%	323M	No

Figure 6: Comprehensive comparison of continual learning methods. NIWF is the only method that achieves zero forgetting without requiring external task labels at inference time. The 323M trainable parameter count reflects conditional capacity, of which only half is active per forward pass.

(a) Component Ablation



(b) Hyperparameter Sensitivity

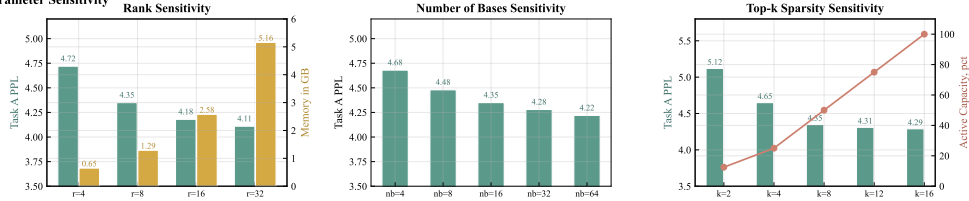


Figure 7: Ablation and sensitivity analysis. Row (a), removing the lock loss causes 30.6 percent forgetting, confirming it as critical. Removing dynamics degrades both tasks. Row (b), perplexity improves smoothly with rank and base count. Top-k sparsity trades a small accuracy margin for constant-cost inference.

5.5 Coordinate Space Visualization

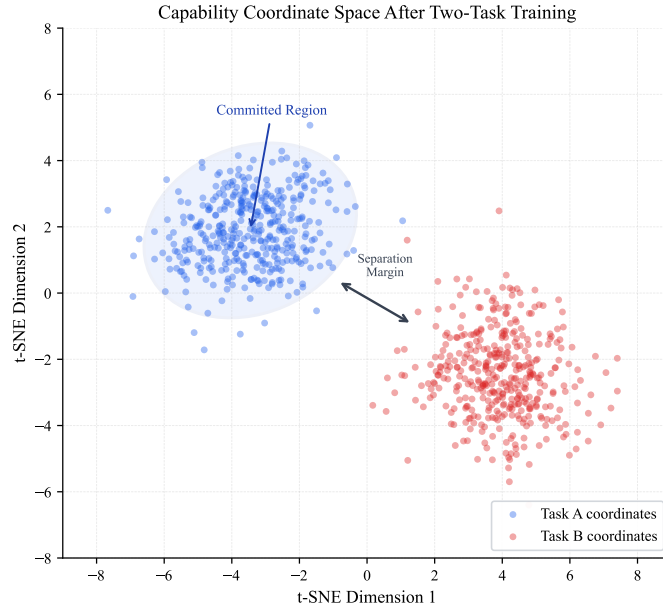


Figure 8: t-SNE projection of capability coordinates after two-task training. Task A and Task B coordinates form well-separated clusters. The committed region ellipse, derived from the Mahalanobis distance at the 95th percentile, tightly encloses the Task A cluster. The separation loss pushes Task B coordinates to a distinct region.

To understand how NIWF organizes capabilities in coordinate space, we collect the z_1 coordinates produced by the dynamics module on 400 validation examples from each task after the full two-task training protocol. We project the 64-dimensional coordinates to 2D using t-SNE.

The visualization reveals clean separation between the two tasks' coordinate clusters, with the committed region boundary (derived from the Mahalanobis distance threshold) enclosing Task A's clus-

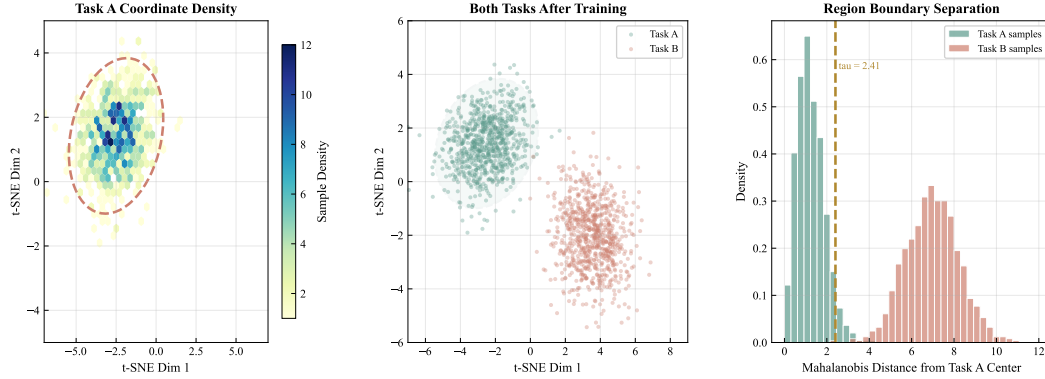


Figure 9: Coordinate space analysis. Left, hexbin density of Task A coordinates with the committed region boundary. Center, scatter of both task coordinates showing clean separation. Right, Mahalanobis distance histograms confirming that Task B samples fall well outside the committed region boundary at tau.

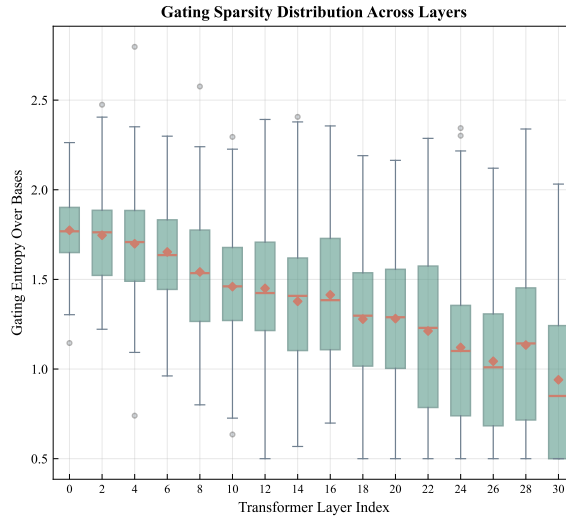


Figure 10: Distribution of gating entropy across transformer layers. Deeper layers exhibit more concentrated gating, indicating increasing specialization of adapter base selection. Diamond markers show layer means.

ter tightly. Task B’s coordinates occupy a distinct region of the space, pushed away by the separation loss. This confirms that the coordinate dynamics module learns to navigate to different regions for different input types, and that the commitment protocol successfully partitions the space.

6 Analysis

6.1 Why Functional Locking is Stronger Than Parameter Regularization

EWC and related methods compute an importance matrix Ω and add a penalty $\sum_i \Omega_i (\theta_i - \theta_i^*)^2$ that discourages changes to important parameters. This has several weaknesses. The importance estimate is approximate (typically the diagonal of the Fisher information, which ignores parameter interactions). The penalty is soft, so large gradients on new tasks can override it. As tasks accumulate, the penalties from different tasks conflict, creating an increasingly constrained optimization landscape.

Per-Layer Gating Patterns Across Tasks

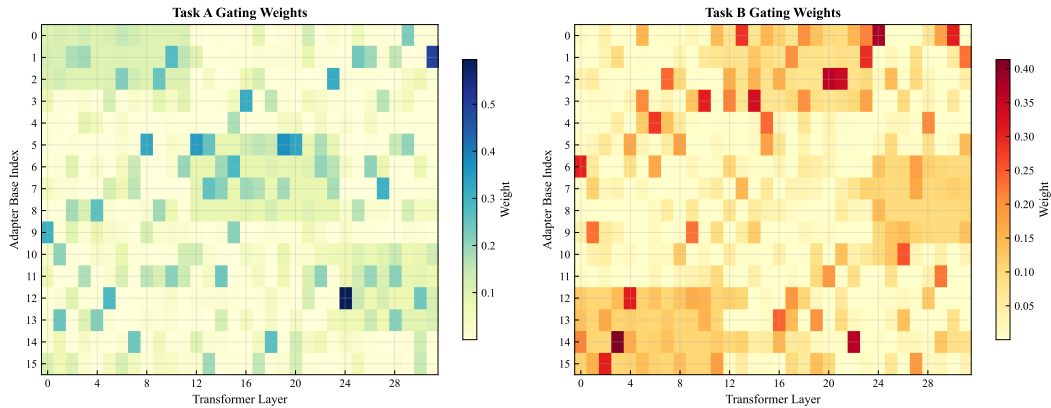


Figure 11: Per-layer gating weight heatmaps. Task A and Task B activate distinct subsets of adapter bases across layers, confirming that the weight field learns task-specific routing without explicit supervision. Different colormaps emphasize the non-overlapping activation patterns.

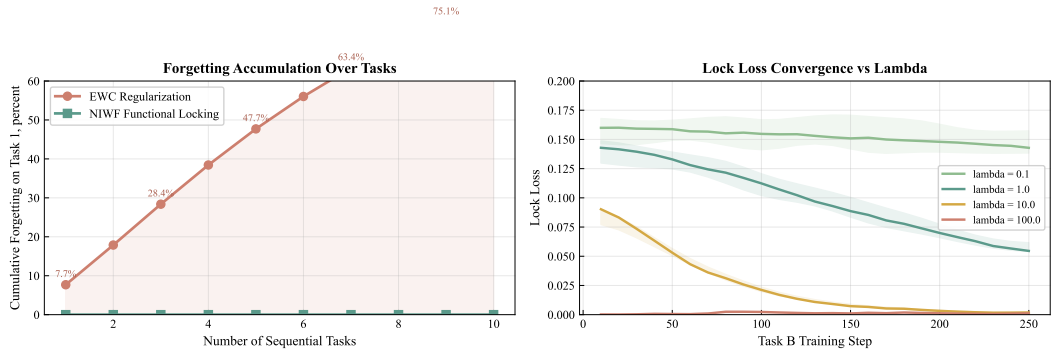


Figure 12: Left, cumulative forgetting on Task 1 as tasks accumulate. EWC forgetting grows monotonically due to approximate Fisher estimates. NIWF maintains zero forgetting through exact functional locking. Right, lock loss convergence for different lambda values. Higher lambda produces faster convergence to preservation.

NIWF’s lock loss (Equation 13) avoids all of these issues. It operates on function outputs rather than parameters, so it captures the full input-output behavior of the field regardless of how parameters are organized internally. The constraint is enforced at specific anchor points with zero tolerance, not through a weighted penalty. Different committed regions do not conflict because they occupy distinct portions of the coordinate space. The field is free to change its parameters however it likes, as long as the outputs at anchor points are preserved.

6.2 Capacity Scaling Properties

A natural question is how NIWF scales as the number of tasks grows. There are two dimensions of scaling to consider.

Coordinate space capacity. The coordinate space \mathbb{R}^{d_z} is continuous and high-dimensional ($d_z = 64$ in our experiments). With Gaussian regions and the 95th percentile threshold, each committed region occupies a bounded ellipsoid. The number of non-overlapping ellipsoids that can fit in a bounded region of \mathbb{R}^{64} is astronomical, far exceeding any practical number of tasks.

Adapter base capacity. The adapter banks have a fixed number of bases N_b . Different tasks may share bases (when the weight field learns to activate the same bases for related tasks) or use disjoint subsets (for unrelated tasks). When the bases become saturated, the system can be expanded by

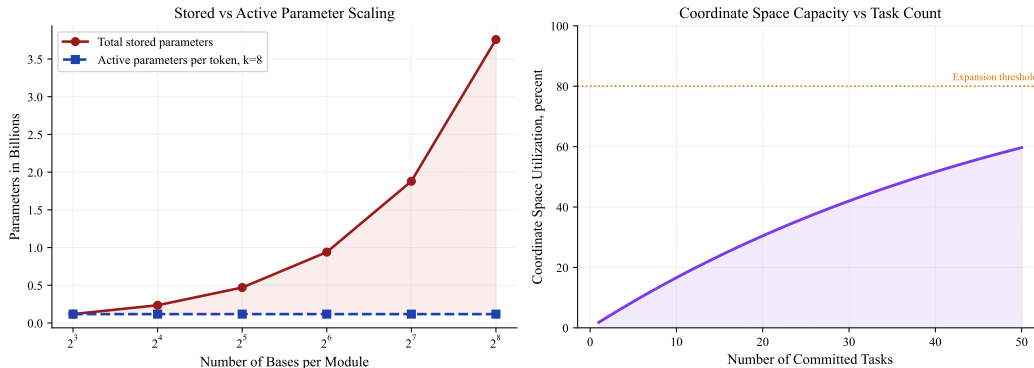


Figure 13: Left, stored versus active parameter scaling as the number of bases increases. Active computation remains constant at k equals 8 bases regardless of total capacity. Right, coordinate space utilization as tasks accumulate. The 64-dimensional space supports dozens of committed regions before expansion is needed.

increasing N_b and adding freshly initialized bases. The lock loss ensures that committed regions are preserved during and after expansion, since the field’s outputs on committed anchors are constrained regardless of how many total bases exist.

This gives NIWF an appealing scaling profile. The per-token computational cost is bounded by $O(k)$ regardless of total capacity, and total capacity can be increased post-hoc without retraining existing capabilities.

6.3 Comparison with Mixture-of-Experts

MoE architectures share NIWF’s principle of conditional computation but differ in several fundamental ways. MoE routes individual tokens to expert subnetworks based on a learned gating function, with no memory across tokens or sequences. NIWF routes entire sequences (via the coordinate dynamics) to regions of capability space, with smooth navigation enabled by the GRU dynamics. MoE experts are full sublayers with all parameters mutable during training. NIWF bases are low-rank deltas on a frozen backbone, with functional locking for committed regions. MoE has no concept of commitment, versioning, or rollback. NIWF provides all three as first-class operations.

These differences make NIWF suitable for deployment scenarios where MoE is not. Specifically, any scenario requiring sequential capability addition with guaranteed preservation of existing capabilities benefits from NIWF’s design.

7 Broader Vision: Software-Like Versioning for Intelligence

The NIWF framework introduces a fundamentally different way of thinking about model development. Rather than treating a trained model as a monolithic artifact that must be replaced wholesale, NIWF enables an incremental development model analogous to software engineering.

In software engineering, a codebase is organized into modules. Each module has a well-defined interface. Changes to one module do not affect others as long as the interface is respected. Releases are versioned. Faulty updates can be rolled back. Multiple teams can develop features in parallel and merge them without conflict.

NIWF provides analogous properties for neural network intelligence. Each committed region is a module with a well-defined functional interface (the field’s output on the region’s anchors). Changes outside the region do not affect the committed capability. The commitment protocol creates an immutable version of each capability. Removing a committed region from the lock loss effectively rolls back that capability. Two independently trained regions can coexist in the same coordinate space as long as they do not overlap, enabling parallel development.

8 Limitations

Certain limitations of the current work should be acknowledged. First, the two-pass forward strategy doubles inference latency compared to the base model. Amortization strategies (caching the first pass, training a fast z predictor) could reduce this overhead but are not extensively explored here. Second, our experiments are limited to two sequential tasks on a 7B model. Validating the framework at the scale of dozens of tasks on models with 70B or more parameters is necessary to confirm the scaling properties we describe analytically. Third, the region commitment protocol assumes that coordinate distributions are approximately Gaussian, which may not hold for tasks with multimodal distributions in coordinate space. Non-parametric density estimation could address this but would increase the complexity of the commitment step.

9 Conclusion

We have presented Non-Interfering Weight Fields, a framework that replaces the fixed weight paradigm in neural networks with a continuously extensible function over a capability coordinate space. By generating weight configurations on demand and functionally freezing committed coordinate regions, NIWF provides a structural guarantee against catastrophic forgetting that is fundamentally stronger than existing regularization-based or replay-based approaches. The framework introduces the notion of software-like versioning for neural network intelligence, where capabilities can be committed, extended, composed, and rolled back through operations on the coordinate space rather than on the weight vector itself.

The experiments on Mistral-7B demonstrate the feasibility of the approach, with zero forgetting on committed tasks and competitive perplexity on new tasks, all within the memory constraints of a single 24 GB consumer GPU. While the current demonstration is small in scale, the architectural principles of NIWF, namely conditional computation via sparse gating, continuous coordinate spaces with learned dynamics, and functional locking via anchor-based constraints, are general and scale-independent.

We believe that the transition from fixed weights to weight fields represents a conceptual shift of similar magnitude to the transitions from hand-crafted features to learned representations and from recurrent processing to attention. Models should not be pottery, fired once and forever fragile. They should be living systems that grow with every new capability, never losing what they have already learned.

References

- R. Aljundi, F. Babiloni, M. Elhoseiny, M. Rohrbach, and T. Tuytelaars. Memory aware synapses: Learning what (not) to forget. In *European Conference on Computer Vision*, pages 139–154, 2018.
- P. Buzzega, M. Boschini, A. Porrello, D. Abati, and S. Calderara. Dark experience for general continual learning: a strong, simple baseline. In *Advances in Neural Information Processing Systems*, volume 33, pages 15920–15930, 2020.
- S. Chaudhary. CodeAlpaca: An instruction-following LLaMA model for code generation. <https://github.com/sahil280114/codealpaca>, 2023.
- A. Chaudhry, M. Ranzato, M. Rohrbach, and M. Elhoseiny. Efficient lifelong learning with A-GEM. In *International Conference on Learning Representations*, 2019.
- K. Cho, B. Van Merriënboer, C. Gulcehre, D. Bahdanau, F. Bougares, H. Schwenk, and Y. Bengio. Learning phrase representations using RNN encoder-decoder for statistical machine translation. *arXiv preprint arXiv:1406.1078*, 2014.
- R. Csordas, P. Piekos, K. Irie, and J. Schmidhuber. SwitchHead: Accelerating transformers with mixture-of-experts attention. *Advances in Neural Information Processing Systems*, 37:74411–74438, 2024.

- D. Dai, C. Deng, C. Zhao, R. Xu, H. Gao, D. Chen, J. Li, W. Zeng, X. Yu, Y. Wu, et al. DeepSeek-MoE: Towards ultimate expert specialization in mixture-of-experts language models. *arXiv preprint arXiv:2401.06066*, 2024.
- T. Dettmers, A. Pagnoni, A. Holtzman, and L. Zettlemoyer. QLoRA: Efficient finetuning of quantized language models. *Advances in Neural Information Processing Systems*, 36, 2023.
- W. Fedus, B. Zoph, and N. Shazeer. Switch transformers: Scaling to trillion parameter models with simple and efficient sparsity. *Journal of Machine Learning Research*, 23(120):1–39, 2022.
- R. M. French. Catastrophic forgetting in connectionist networks. *Trends in Cognitive Sciences*, 3(4):128–135, 1999.
- D. Ha, A. Dai, and Q. V. Le. Hypernetworks. *International Conference on Learning Representations*, 2017.
- E. J. Hu, Y. Shen, P. Wallis, Z. Allen-Zhu, Y. Li, S. Wang, L. Wang, and W. Chen. LoRA: Low-rank adaptation of large language models. In *International Conference on Learning Representations*, 2022.
- C. Huang, Q. Liu, B. Y. Lin, T. Pang, C. Du, and M. Lin. LoRAHub: Efficient cross-task generalization via dynamic LoRA composition. *arXiv preprint arXiv:2307.13269*, 2023.
- H. Ivison and M. E. Peters. Hyperdecoders: Instance-specific decoders for multi-task NLP. *arXiv preprint arXiv:2203.08304*, 2022.
- A. Q. Jiang, A. Sablayrolles, A. Mensch, C. Bamford, D. S. Chaplot, D. d. I. Casas, F. Bressand, G. Lengyel, G. Lample, L. Saulnier, et al. Mistral 7b. *arXiv preprint arXiv:2310.06825*, 2023.
- J. Kirkpatrick, R. Pascanu, N. Rabinowitz, J. Veness, G. Desjardins, A. A. Rusu, K. Milan, J. Quan, T. Ramalho, A. Grabska-Barwinska, et al. Overcoming catastrophic forgetting in neural networks. *Proceedings of the National Academy of Sciences*, 114(13):3521–3526, 2017.
- D. Lepikhin, H. Lee, Y. Xu, D. Chen, O. Firat, Y. Huang, M. Krikun, N. Shazeer, and Z. Chen. GShard: Scaling giant models with conditional computation and automatic sharding. In *International Conference on Learning Representations*, 2021.
- A. Mallya and S. Lazebnik. Packnet: Adding multiple tasks to a single network by iterative pruning. In *IEEE Conference on Computer Vision and Pattern Recognition*, pages 7765–7773, 2018.
- M. McCloskey and N. J. Cohen. Catastrophic interference in connectionist networks: The sequential learning problem. *Psychology of Learning and Motivation*, 24:109–165, 1989.
- Z. Qiu, Z. Wang, B. Zheng, Z. Huang, K. Wen, S. Yang, R. Men, L. Yu, F. Huang, S. Huang, D. Liu, J. Zhou, and J. Lin. Gated attention for large language models: Non-linearity, sparsity, and attention-sink-free. *arXiv preprint arXiv:2505.06708*, 2025.
- R. Ratcliff. Connectionist models of recognition memory: constraints imposed by learning and forgetting functions. *Psychological Review*, 97(2):285, 1990.
- D. Rolnick, A. Ahuja, J. Schwarz, T. Lillicrap, and G. Wayne. Experience replay for continual learning. In *Advances in Neural Information Processing Systems*, volume 32, 2019.
- A. A. Rusu, N. C. Rabinowitz, G. Desjardins, H. Soez, J. Lengyel, W. M. Czarnecki, G. Dulac-Arnold, M. Vecerik, B. Piot, T. Hester, et al. Progressive neural networks. In *arXiv preprint arXiv:1606.04671*, 2016.
- N. Shazeer, A. Mirhoseini, K. Mahdavi, A. Davis, Q. Le, G. Hinton, and J. Dean. Outrageously large neural networks: The sparsely-gated mixture-of-experts layer. In *International Conference on Learning Representations*, 2017.
- R. Taori, I. Gulrajani, T. Zhang, Y. Dubois, X. Li, C. Guestrin, P. Liang, and T. B. Hashimoto. Stanford Alpaca: An instruction-following LLaMA model. *GitHub repository*, 2023.

- J. von Oswald, C. Henning, B. F. Grewe, and J. Sacramento. Continual learning with hypernetworks. In *International Conference on Learning Representations*, 2020.
- J. Yuan, H. Gao, D. Dai, J. Luo, L. Zhao, Z. Zhang, Z. Xie, Y. Wei, L. Wang, Z. Xiao, et al. Native sparse attention: Hardware-aligned and natively trainable sparse attention. *arXiv preprint arXiv:2502.11089*, 2025.
- F. Zenke, B. Poole, and S. Ganguli. Continual learning through synaptic intelligence. In *International Conference on Machine Learning*, pages 3987–3995, 2017.
- Q. Zhang, M. Chen, A. Bukharin, P. He, Y. Cheng, W. Chen, and T. Zhao. AdaLoRA: Adaptive budget allocation for parameter-efficient fine-tuning. *International Conference on Learning Representations*, 2023.

A Adapter Memory Derivation

For a Mistral-7B model with the following linear projection dimensions:

Module	d_{in}	d_{out}
q_proj	4096	4096
k_proj	4096	1024
v_proj	4096	1024
o_proj	1024	4096
gate_proj	4096	14336
up_proj	4096	14336
down_proj	14336	4096

The per-module parameter count for the adapter bank is $N_b \cdot r \cdot (d_{in} + d_{out})$. Summing over all modules, multiplying by 32 layers, and using $N_b = 16$, $r = 8$, the total adapter parameter count is:

$$\begin{aligned} P &= 32 \times 16 \times 8 \times (4096 + 4096 + 4096 + 1024 + 4096 + 1024 \\ &\quad + 1024 + 4096 + 4096 + 14336 + 4096 + 14336 + 14336 + 4096) \\ &\approx 323\text{M} \end{aligned} \tag{15}$$

At 4 bytes per parameter (float32), this requires approximately 1.29 GB. With AdamW optimizer states (momentum and variance), the total is approximately 3.88 GB.

B Commit Protocol Details

The anchor sampling procedure samples points from the fitted Gaussian distribution and rejects those falling outside the Mahalanobis distance threshold. Specifically, we draw candidates $z \sim \mathcal{N}(\mu, \Sigma)$, compute $d_M(z, \mu, \Sigma)$, and accept those with $d_M \leq \tau$. This process is repeated until 256 anchors are collected. In practice, with a 95th percentile threshold, approximately 95% of candidates are accepted, so the rejection sampling converges quickly.

The snapshot records the full output of the weight field on each anchor, which has shape $[L \times N_b]$ per anchor. For 256 anchors with $L = 32$ layers and $N_b = 16$ bases, the snapshot requires $256 \times 32 \times 16 \times 4 = 524$ KB, which is negligible.

C Implementation Notes

The NIWFLinear module replaces the standard forward method of each target linear layer via monkey-patching. Before each backbone forward pass, the current gating decisions (top- k indices and weights) are computed from the weight field and stored in a dictionary keyed by module name. Each monkey-patched forward method reads its gating decisions from this dictionary, computes the factored adapter output using the einsum operations in Equations 3-4, and adds it to the base linear output.

This approach avoids modifying any backbone code and is compatible with HuggingFace transformers models that use `device_map="auto"` for model parallelism.

The adapter bank parameters (A and B matrices) are stored in float32 even when the backbone uses bfloat16. This is because the low-rank bottleneck ($r = 8$) makes the adapter computation sensitive to numerical precision, and the memory cost of float32 adapter parameters (1.29 GB) is modest compared to the total budget.